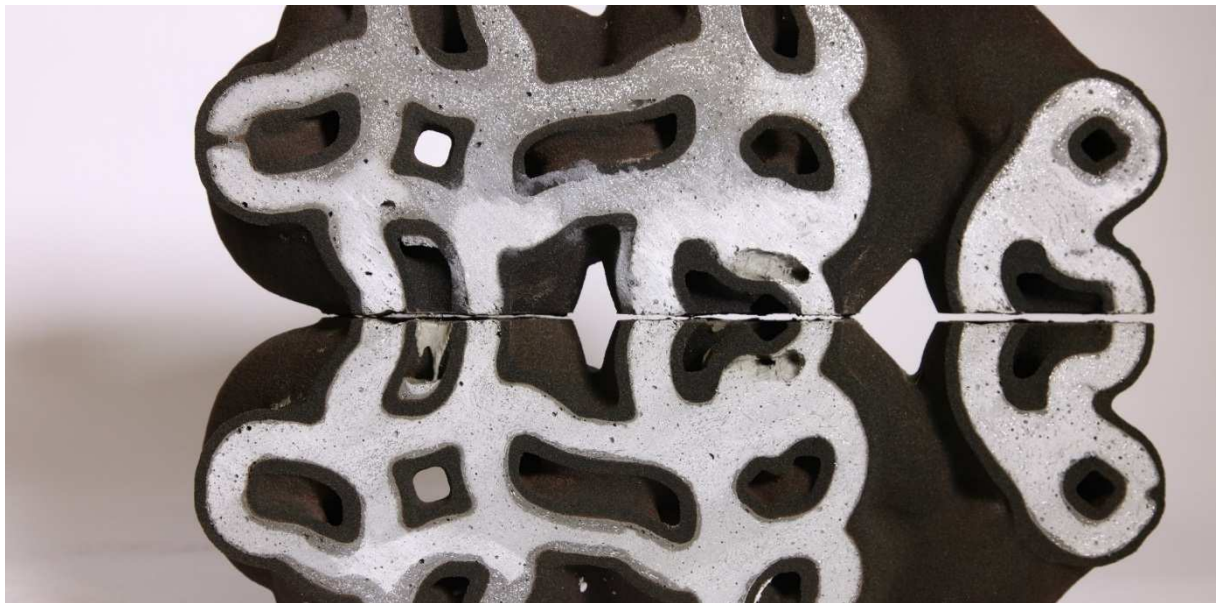


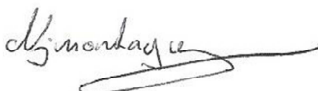
# 3D Sand-Printed High Performance Fibre-Reinforced Concrete Hybrid Structures



*Supervisors:*  
Nicolas Ruffray  
Mathias Bernhard

*Students:*  
Felix Stutz  
Neil Montague de Taisne

06. Juni 2016

Felix Stutz	Neil Montague de Taisne
F. Stutz	

# Index

1	Introduction.....	4
2	Materials and methods.....	5
2.1	Materials.....	5
2.2	Methods.....	8
2.2.1	Mixing procedures.....	8
2.2.2	Measurement methods.....	8
3	Results and discussion.....	13
3.1	Finding a working mix for HPFRC.....	13
3.2	Workability and mechanical properties of HPFRC.....	13
3.3	Mechanical properties of printed sand.....	22
3.4	Interplay of printed sand and water.....	23
3.5	Casting of prototypes for the wished end-product.....	27
4	Conclusion.....	31
5	References.....	33
6	Appendix.....	35

## Abstract

The feasibility of hybrid structures made of 3D sand-printed formworks and high-performance fibre-reinforced concrete was investigated in this thesis. A first suitable mix was found. Direct links between fibre factor, workability, and strength of the high performance fibre reinforced concrete, enabling predictions, could be established. The investigation of the high porosity and sorptivity of the 3D sand-printed formwork and loss of cohesion when in prolonged contact with water, showed that these problems could either be solved by applying an epoxy coating, or the porosity might be also seen as a potential advantage (possibility for entrapped air to escape the formwork). Finally, a table was designed to showcase the potential of this technology for producing ceiling elements.

## Acknowledgements

We would like to express our deepest gratitude to the people who made it possible to write this thesis:

1. Prof. Dr. Robert J. Flatt, who offered us the opportunity to participate in this explorative effort in digital fabrication and brought very insightful critical input,
2. Prof. Benjamin Dillenburger, who put at our disposition the resources of the chair for Digital Building Technologies (DBT), and for his valuable advices,
3. Dr. Timothy Wangler, whose valuable input helped us to orient our efforts and carry through this thesis in an efficient manner, and for organising the needed materials,
4. Dr. Emanuel Denarié from EPFL for his expertise and providing the basis of the mix that was used throughout the thesis,
5. Our supervisor, Nicolas Ruffray, who through his energy, knowledge, advice, and high overall readiness to help, was a critical element in the process of finishing this thesis,
6. Mathias Bernard, for his precious help in design, organisation, and highly contagious enthusiasm for the project,
7. Kwon Hyunchul, for introducing us to the Rhino software, Grasshopper and Millipede for Rhino,
8. Lex Reiter, for his out-of-the-box advices that led us to look more in depth and more critically at some experimental results,
9. Andrei Jipa, for his refreshing enthusiasm, help, and beautiful pictures,
10. Heinz Richner, for helping in the lab with his technical know-how,
11. Thibault Demoulin, for performing some tests for us,

and the rest of the teams of PCBM (Physical Chemistry of Building Materials) at D-BAUG and DBT (Digital Building Technology) at D-ARCH at the Swiss Federal Institute of Technology Zurich.

## Abbreviations

SP	Superplasticiser
DE/C	SP dry extract to cement weight ratio
HPFRC	High performance fiber-reinforced concrete
$f_{ar}$	Fibre aspect ratio
$f_f$	Fibre factor
$l_f$	Fibre length
$d_f$	Fibre width
$V_{fib}$	fibre volume
$V_M$	Matrix volume
$V_{tot}$	Total volume (Matrix + Fibres)
W/C – ratio	Water/Cement ratio
W/B - ratio	Water/Binder ratio
$V_f$	Fibre volume fraction

# 1 Introduction

Building with concrete has the major advantage that due to its workability in the non-hardened state it can be cast to various shapes. Downside of this advantage is the need for preparation of the formworks, which is a very costly process. Each piece of – often wooden - formwork has to be cut and treated prior to casting. The costs rise very rapidly when complicated details have to be integrated, as a lot of smaller pieces of formwork need to be prepared, which implies a high workload. Additionally, this process produces a high amount of waste, as the wood tends to degrade or can't be used again due to its specific cut.

Rationalisation efforts have been made in the last decades with the usage of precast and semi-precast elements, using for instance metal formworks in controlled environments instead of the hardly controllable environment of the building site. These formworks are more durable, more precise, and do not degrade as fast, and enable among other things a better control of the setting of the concrete, better quality of the surfaces, and a higher accuracy of the shape. On the other hand, this method does not enable either to produce in a cost-efficient way complex geometrical shapes, and as the elements have to be transported to the building site the elements cannot be too massive.

3D-sand printing, which is a technology this bachelor thesis relies upon, enables the creation of silica sand moulds of virtually any shape, with high complexity and a resolution between 300 and 600 dpi [1]. As a consequence of the production methods, the *costs are not dependent on the intricacy of the desired end-product, but only on its size*. These sand elements, consisting of silicate sand, hold together by a binder, were originally developed to be used in the machine industry to create formworks for metallic parts. They can however for the moment not be used as structural elements themselves, as the compressive and tensile strength of the material are very low: preliminary tests done by Tim Wangler and Mathias Bernard at ETH Zurich delivered an average cube compressive strength of around 8.5 MPa and a bending strength of around 3 MPa (Appendix, Figure A 3 and Figure A 4).

*An idea would hence be to print such elements as formworks and fill them with reinforcing high performance fibre-reinforced concrete (HPFRC).* This produced hybrid structure would have hence following benefits among others:

- High complexity possible for the details of the sand-printed surface of the structural elements,
- High complexity possible for the overall structural shape (e.g., twisted columns with holes),
- Lighter structures through the usage of topologically optimised structural elements,
- High aesthetic values and individual customized structures,
- Relatively cheap production procedure for high complexity,
- Thinness of the structure through high performance of the concrete,
- Sufficient ductility.

This bachelor thesis is part of a first explorative effort aimed at obtaining information about the feasibility of this idea and possible directions. A milestone of this effort would be the production of a table using this technology, as to show its possibilities, but it could optimally also be used, e.g., as a small-scale model for a ceiling element.

Following steps have been gone through as part of this thesis, with the goal of obtaining more data:

- Finding a good base mix for HPFRC that could be improved to suit the needs of the project,
- Optimise the found mix for workability and strength. If possible obtain strain-hardening for the mix, as it would deliver high ductility for built structural elements,
- Investigate the interplay of the printed sand and added water / water contained in the concrete, as it had been observed during preliminary testing that the printed sand seems to be very porous, tends to absorb water, and loses cohesion when in prolonged contact with water,
- Casting of prototypes for the wished end-product - a table element serving as model for a ceiling element - and realisation of said product.

After a short presentation of the materials and the methods, this thesis will continue with a presentation of the results and discussion of these results, and finally end with a short conclusion, indicating possible future research directions for this technology.

## 2 Materials and methods

### 2.1 Materials

The materials used for all concrete mixes and samples can be seen in Table 1.

Material	Name	Producer
<b>Cement</b>	Durabat X-trem - CEM I 52.5 N SR 5 PM-CP2	Lafarge
<b>Sand</b>	0.1-0.45 mm	Baubedarf
<b>Silica Flour</b>	K6	Carlo Bernasconi AG
<b>Silica Fume</b>	Elkem Grade 971-U	Elkem
<b>Superplasticizer</b>	MasterGlenium ACE 30 MasterGlenium SKY 561	BASF BASF

Table 1: Materials used for the concrete matrix.

### Fibres

The used steel fibres are fully straight without hooked ends. The geometric properties of the steel fibres can be seen in Table 2. The mechanical properties as well as the rheology of HPFRC are linked not only to the fibre content but also to the geometric properties of the fibres. In order to be able to compare the rheology and mechanical properties of different concrete mixes, the geometry of the fibres and the fibre content of the mix are taken into account using the fibre aspect ratio (Equation 1) and fibre factor (Equation 2).

The fibre aspect ratio  $f_{ar}$  is a simple geometric value and useful to compare the properties of different individual fibre types. The fibre factor  $f_f$  takes the geometry and amount of fibres into account.

$$f_{ar} = \frac{l_f}{d_f} [-] \quad (1)$$

$$f_f = f_{ar} \cdot \frac{V_f}{V_{tot}} [-] \quad (2)$$

Steel Fibres	Length [mm]	Width [mm]	Aspect ratio [-]	Producer
Type 1	6	0.15	40	Dramix
Type 2	10	0.16	62.5	Dramix
Type 3	13	0.16	81.3	Dramix

Table 2: Steel fibres used as fibre reinforcement for the concrete.

## HPFRC

High Performance Fibre Reinforced Concretes typically have a dense and fine granular matrix containing small and especially hard aggregates, low water/binder ratios and high amounts of silica fume and superplasticizer, leading to an extremely compact matrix. The concrete matrix of the mixes used in this thesis did not exceed 100 MPa and therefore was classified as high performance fibre reinforced concrete (HPFRC).

All HPFRC formulas used can be found in the appendix (Figure A 1). The volume fraction of the fibres was calculated as the volume of the fibres divided by the total volume (Equation 3). The total volume is equal to the volume of the fibres plus the volume of the concrete matrix.  $V_{fib}$  was calculated as the mass of the fibres divided by the density of the fibres  $\rho_{fib} = 7880 \frac{kg}{m^3}$  (Equation 4). The volume of the matrix  $V_m$  was calculated with Equation 5.

$$V_f = \frac{V_{fib}}{V_{tot}} [-] \quad (3)$$

$$V_{fib} = \frac{m_{fib}}{\rho_{fib}} [m^3] \quad (4)$$

$$V_m = \frac{m_{tot}}{\rho_{tot}} - V_{fib} [m^3] \quad (5)$$

$V_f$ : Fibre volume fraction [-]

$V_{fib}$ : Fibre volume [ $m^3$ ]

$V_m$ : Matrix volume [ $m^3$ ]

## Superplasticisers (SPs)

Both applied superplasticizers MasterGlenium ACE 30 and MasterGlenium Sky 561 are polycarboxylate ether-based (PCE) [2]. These polymers are characterised through an anionic backbone and positively charged side chains (Figure 1). The negatively charged backbone sticks to the positively charged cement particles while the side chains reach into the solution. The positively charged side chains lead to a repulsion of the cement particles and an increased distance between them [3] (Figure 2). The latter strongly reduces the van der Waals forces and therefore increases the flowability of the concrete.

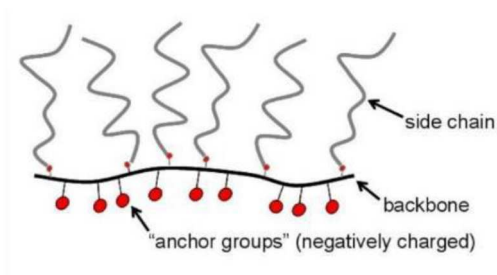


Figure 1: PCE-based polymer [4].

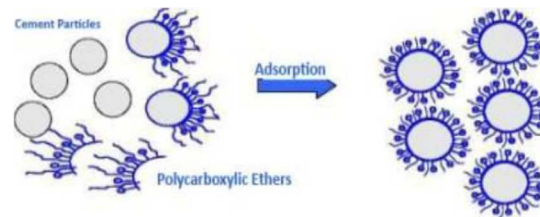


Figure 2: Adsorption of the polymers to cement particles [5].

Even though the general mechanisms of action are the same for PCE based superplasticizers, the characteristics of the particular products still can vary strongly as there is a large amount of parameters, which can be varied during manufacturing. This also brings the opportunity of finding or choosing well-adapted superplasticisers for concrete with specific requirements. The most important parameters are [2]:

- The type of monomers used for the backbone and the amount of negative loads
- The length of the backbones
- The composition of the side chains
- The length of the side chains in respect to the backbones

### 3D sand-printed elements and binders

3D sand-printing is a rather new technology but it has already been used for producing formworks for metal casting [1]. It shows several advantages [1]:

- high contour accuracy with high resolutions of 300-600 dpi.
- complex geometries with undercuts can be produced
- costs don't rise with increased complexity but only with the amount of used sand.

This technology today thus offers an economic alternative for producing complex metal parts with low quantities. But applications might also be possible for architecture.

The process of 3D sand-printing can be seen in Figure 3. The basis for the printing process is a CAD model of the element that should be printed. On the building platform of the printer a most commonly 250-400  $\mu\text{m}$  thick layer of sand is applied and smoothed out. The printer applies binder according to the section planes from the CAD model. Afterwards the building platform is lowered and the next layer of sand is applied and smoothed out. These steps are repeated until the whole element is printed. At the points where no binder has been applied, the sand remains loose and can after completion of the printing process be brushed off or removed trough compressed air.

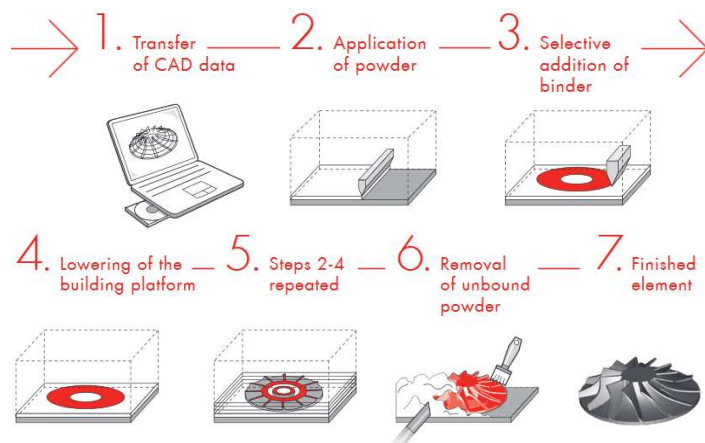


Figure 3: Process of 3D sand-printing. [1]

The sand printed elements used for this thesis were designed by the Chair for Digital Building Technology (DBT) at the Department of Architecture (D-ARCH) at ETH Zurich, and printed by Christenguss AG (Industriestrasse 44, 8962 Bergdietikon, Switzerland). The elements are all made of silica sand, and two different binders, a furanic and a phenolic one, were used. Elements using one binder or the other can be distinguished



through their appearance, as the furanic based binder appears dark black and the phenolic light brown.

## 2.2 Methods

### 2.2.1 Mixing procedures

The mixings were produced using a Hobart A200N mixer. The formulation of the produced concrete mixes can be seen in Table 3, the description of the mixing process can be found in Table 3.

Step	Procedure	Remarks	Time at the end of the step
1	Mix the dry components on speed 1 for 5 min	Dry components = cement, silica flour, silica fume, sand	5 min
2	Add the water	Let the mixer run during this procedure	5.5 min
3	Mix on speed 1 for 1 min		6.5 min
4	Add superplasticiser	Let the mixer run during this procedure	7 min
5	Mix on speed 1 for 6 min, or until change of rheology if it hasn't occurred yet at that time		13 min (+ t min)
6	Mix on speed 2 for 5 min		18 min (+ t min)
7	Stop the mixer and add half of the fibres (1 min)	Restart the mixer after the minute	19 min (+ t min)
8	Mix on speed 1 for 30s		19.5 min (+ t min)
9	Stop the mixer and add the other half of the fibres (1 min)	Restart the mixer after the minute	20.5 min (+ t min)
10	Mix on speed 1 for 3 min		23.5 min (+ t min)

Table 3: Mixing procedure for the HPFRC.

### 2.2.2 Measurement methods

#### Mini-slump flow

A so called “mini-slump flow test” has been used to describe the flowing behaviour of the concrete. Further mentions of “slump flow” or “slump flow diameter” refer to the test and diameter measured using the “mini-slump flow test”. The dimensions of the used mould can be found in Table 4. As shown by [6] there is a good correlation between the mini slump flow test and the normal and larger, standardized slump flow measurements.

The process of obtaining the slump flow diameter is as follows:

- Put the dry mould on a dry glass plate,
- Fill the mould right after the mixing (described in 2.2.1), make sure that the surface of the concrete is at the same height as the upper limit of the mould,
- Lift the mould slowly, keep it approximately 1 cm above the concrete surface for 10s to let most of the concrete contained in the mould leave it,
- Measure the diameter after 3 min (average of the diameter of two orthogonal directions).

Height	6.0 cm
Radius of bottom section	3.5 cm
Radius of top section	5.0 cm
Volume	344 cm <sup>3</sup>

Table 4: Dimensions of the mini slump flow mould.

### **Dry extract content of the superplasticiser**

An accurate description of the flowing behaviour of the concrete in function of the amount of used superplasticiser was desired. It is important for that point to consider the fact that both superplasticisers contain a part of water and a part of dry extract, which contains the active ingredient. Additionally, this dry extract fraction can vary from canister to canister.

The dry extract is the driving force for increasing the workability, while the water content affects the W/C and W/B ratio. It had thus been decided that the amount of dry extract would be used as a parameter, and the added water content in the mix would be adapted as to have a fixed water-to-binder ratio.

The superplasticiser content has been measured as follows using a KEN MRS 120-3 device:

- Put quartz sand on a small plate,
- Tar the plate in the machine,
- Put a couple of grams of liquid on the sand,
- Close the machine, run it at 105° until weight stabilises (= no more water),
- The dry extract content is then the ratio of the remaining mass to the original mass.

### **Workability with time**

To investigate the decrease of workability with time two batches of the same mix were prepared (formula 13, see Appendix, Figure A 1). The slump flow for both of the batches was performed every 15 min, and every 30 min after 75 min, and stopped when the decreased workability of the concrete would make it difficult to carry out the measurement. The second mix, unlike the first one, was remixed for 1 min on speed 1 on the Hobart A200N before measuring the slump diameter.

### **Isothermal calorimetry**

The hydration reaction of cement is an exothermic reaction. The heat released during the hydration process was measured through a calorimetry test using an I-Cal 8000-2. The used software was CalCommander. The used concrete mix was made according to Formula 12 (see Appendix, Figure A 1), while leaving out steps 7 and 9 of the mixing procedure as no fibres were used in the formula. The moment when the first drop of water touched the dry mix was taken as zero-point for the following time measurements in the calorimeter. Additionally, the elapsed time was measured until the chamber of the calorimeter was closed. The heat release of the hydration was recorded during two days.

### **Bending/compression tests**

The bending and compression tests had been performed using a Walter+Bai FTS Typ 502/4000/100 to measure the 7-day and 28-day strengths.

The prismatic samples had a dimension of 40x40x160mm and were stored after casting and prior to testing in a room with constant temperature (20°) and relative air humidity (95%). For the bending tests 3-point bending was used, with supports at a distance of 100mm. The load was applied exactly in between the supports.

For the compression tests the intact parts of the prisms which underwent a bending test beforehand, were used (See Figure 4). It was assumed that the trajectory of the forces

would be mostly the same as for a traditional cube compression test. As the goal was mainly to compare the samples and get a general idea of the strength instead of delivering very precise results, this approach was assumed to be tolerable.

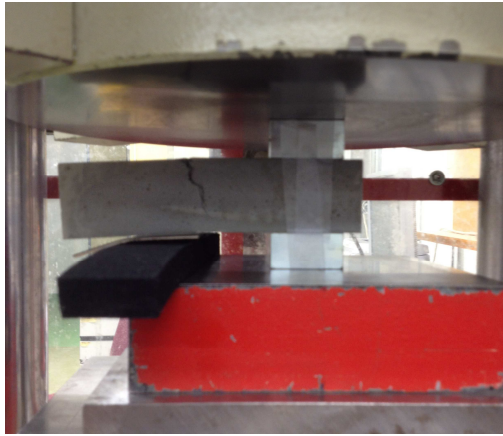


Figure 4: Setup of the compression tests.

### **Total Organic Carbon analysis (TOC analysis)**

A TOC analysis delivers the amount of organic and inorganic carbon in a liquid.

The TOC analysis was performed for 3 sand-printed samples for each binder type (phenolic and furanic), as follows:

- Measurement of the mass of the samples,
- For each sample, prepare ultra-pure water, to put in a clean glass container, with a sample mass to water mass ratio of 1/5,
- Prepare reference containers to measure the TOC of the glass containers,
- Measure the organic and the inorganic carbon with a total organic carbon analyser after 5min, 60min, and 24h for each type of binder.

### **Sorptivity**

The process of the measurement of the sorptivity was the same for each sample:

- The dimensions of the sample base, which will touch the water later in the experiment, were measured using a plastic ruler.
- The sample was clamped in a steel frame and hung on to a scale. It is important that the base of the sample is parallel to the water surface.
- The scale was restored to zero. Therefore, the change in mass of the sample could be measured.
- A bowl of water was placed underneath the sample so that the whole bottom of the sample slightly touched the water.

The measurements with the scale were recorded over time by a connected computer.

Equation 6 was used to draw conclusion about the sorptivity of the samples. It can be seen that the mass of the water normalised by the area is proportional to the square root of the time. The proportional factor is referred to as sorptivity [7].

$$\frac{m_W}{A} = \rho \phi \sqrt{\left( \frac{\gamma_{LV} \cos(\theta)}{2\eta} \cdot r \right)} \cdot \sqrt{t} \quad [7] \quad (6)$$

$m_W$ : Mass of water [m]  
 $A$ : Area of the cross section of the sample [m<sup>2</sup>]  
 $\rho$ : Density of the material [kg/m<sup>3</sup>]  
 $\phi$ : Porosity of the material [-]  
 $\gamma_{LV}$ : Liquid-vapour surface tension [J/m<sup>2</sup>]  
 $\theta$ : Wetting angle of the water/solid interface [°]  
 $\eta$ : Viscosity of the liquid [Pa · s]  
 $t$ : Time [s]

## Porosity measurements

All the sand printed samples used for the porosity measurements were printed using the furan based binder. Three different samples were used:

- Not coated cube
- Cube with epoxy resin coating
- Thin platelet coated with epoxy resin

The latter sample can be considered fully impregnated throughout the entire cross-section because of its thinness.

The porosity was calculated using Equation 7. The bulk density and matrix density were computed by using Equation 8 respectively Equation 9.

$$\Phi = 1 - \frac{\rho_b}{\rho_m} \quad (7)$$

$$\rho_b = \frac{m_s}{V} \quad (8)$$

$$\rho_m = \frac{m_s}{V_s} \quad (9)$$

$$V_s = V - V_p \quad (10)$$

$$V_p = \frac{m_w - m_s}{\rho_{\text{water}}} \quad (11)$$

$V$ : Volume of the sample [m<sup>3</sup>]  
 $\rho_b$ : Bulk density [kg/m<sup>3</sup>]  
 $\rho_m$ : Matrix density [kg/m<sup>3</sup>]  
 $m_s$ : Mass of the dry sample [kg]  
 $\rho_{\text{water}} \approx 1000 \frac{\text{kg}}{\text{m}^3}$ , approximated density of water  
 $V_s$ : Volume of the matrix [m<sup>3</sup>]  
 $V_p$ : Volume of the pores [m<sup>3</sup>]  
 $m_w$ : Mass of the wet sample [kg]

The dry mass  $m_s$  of the sample was measured with a scale and the volume  $V$  was calculated using the dimensions measured with a calliper. The volume of the matrix  $V_s$  can be calculated using Equation 10, the volume of pores  $V_p$  was calculated using Equation 11. For that the wet masses of the samples are needed. The samples underwent following wetting procedure so that the open pores would be infiltrated by the water.

First the sample was placed in a vacuum desiccator and a vacuum pump was installed in the desiccator. A tube connected to the desiccator was submerged in water and the valve to the desiccator was slowly opened so that water would flow into the desiccator. As soon as the sample was about 2 cm underneath the water surface the valve was slowly closed and the atmospheric pressure was slowly restored through reopening the valve. The rising pressure was pressing the water inside the porous network of the sample. After two weeks the samples were taken out of the desiccator and weighed.

## Concrete casting tests

Two experimental set-ups were performed to have an idea of the minimal required tube diameters of the sand-printed elements and their geometric constraints.

The first set-up can be seen in Figure 5. The sand printed elements were vertically filled. This experiment was performed for each fibre type and once without steel fibres. The used concrete mixes were Formula 8, Formula 13, Formula 14 and Formula 12 (see Appendix, Figure A 1). The mixes were chosen because Formulas 8 and 13 have the same slump flow and Formula 13 a slightly lower slump flow. The results can be seen in section 3.5.

The second set-up consisted of L-shaped tubes which all have a diameter of 2 cm but varying angles. The test was performed with the concrete mixes according to Formula 8, 13 and 14.



Figure 5: Straight sand printed tubes filled with concrete. Length: 50cm. Diameters from left to right [mm]: 5, 7.28, 10.14, 13.73, 18.22, 23.85, 30.92, 39.77, 50.87.

## Wished end-product, table element

Two table elements were designed by the chair of digital building technology (DBT). The geometries of both table elements are the same and had been designed through topological optimization with the software Abaqus. The dimensions are 2m x 1m x 0.18m. The second table lies unlike the first table in a bed of loose sand, which itself is enclosed by a thin-walled sand-printed mould. As the 3D-printed sand has a low flexural and compressive strength (see Appendix, Figure A 3 and Figure A 4) the bed of loose sand should distribute the pressure through the fresh concrete on the formwork evenly, and therefore reduce the stress on the formwork.

For the table elements the concrete mix (Formula 13) had to be upscaled. For the mixing process a Collomatic 65/2 K-3 was used. The mixing process was performed as mentioned in section 2.2.1 with the exception that speed 1 was considered to be 50% of the maximum speed and speed 2 was at 100%, maximum speed. As the Collomatic was too small to produce enough concrete in one batch, three batches had to be produced. As the mixing process for one batch takes 23.5 min, it was decided to mix two concrete batches in advance to avoid interrupting the casting process and therefore to avoid construction joints or cold joints in the table element. The third batch was mixed as the table was casted. The slump flow was measured after each mixing to monitor the batch.

## **3 Results and discussion**

### **3.1 Finding a working mix for HPFRC**

The first goal of the thesis was to find a HPFRC mix fulfilling the minimum requirements in terms of workability, as the concrete would have to be cast in complex formworks. A mix and mixing procedure suggested by Emmanuel Denarié of EPFL were used as a basis for preliminary testing (for formula see Appendix, Figure A 6), their adapted version (for the purpose of this application), keeping same mixing procedure, can be found in section 2.1.

First successful testing delivered a slump diameter of 14.75 cm (compared to 23-28cm with the final mixes using the same SP, see section 3.2), which is too low. A second test, when decreasing  $V_f$  by 41% and increasing the SP content by 25% delivered a satisfying slump flow of 23.75 cm. Both mixes can be seen in the Appendix (Figure A 1, formulas 2 and 3)

With a working mix at hand, focus was then set on the testing and optimisation of the workability and strength.

### **3.2 Workability and mechanical properties of HPFRC**

The first working mix was usable, but could still be improved. Decision was made to try and find an optimal superplasticiser content, and find a relationship between the content of SP dry extract and the slump diameter.

#### **Optimal superplasticiser content for the mix**

The addition of superplasticiser to concrete improves the workability of a concrete mix, but on the other hand adding too much is not cost-efficient as SPs are relatively expensive. A goal was hence to find a maximal superplasticiser content for the mix (presented in 2.1) for which no more benefit in terms of flowability (measured by the slump diameter) could be noticed.

For that, it was decided to measure the slump diameter of the concrete mix (with a realistic amount of fibres) when changing the superplasticiser dry extract content, the water-to-binder ratio was being set to a constant 0.309. After interpretation of the results, the amount would be either increased or decreased until a tendency for the results could be observed.

Starting point was a DE/C (SP dry extract to cement weight ratio) of 2.5%, and it was first decided to increase in steps of 0.5%. After two trials, at 3.5% of dry extract, a tendency could be observed (apparent maximum between 2.5% and 3%), which was then refined by a tests with 2.75% and one with 4% (to check if the trend continued as expected). The resultant curve can be seen in Figure 6. The formulas can be found in the appendix, Figure A 1, formulas 3-7.

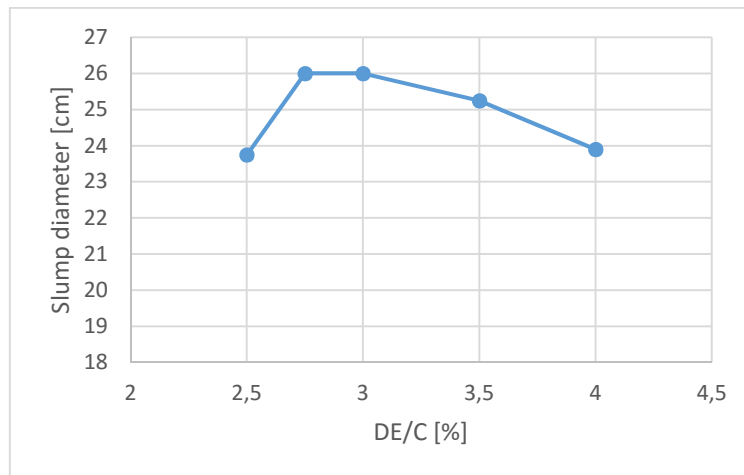


Figure 6: SP dry extract content vs. slump diameter, SP=BASF MasterGlenium ACE 30.

As a maximum for the slump flow was obtained for a DE/C of 2.75% and 3%, it was decided to use 2.75%, which would use less SP and imply a lower delaying of the setting time for the concrete. This DE/C would be used for the rest of the thesis. As a result of that, the water content would also be set fix.

It has to be noted, that during the experiments a non-negligible reduction in slump flow was measured when mixing for two additional minutes, after ending of the standard procedure (around 2cm less compared to the anomalous ~24cm measured before). Repeating the mixing again with two additional minutes, reduced again significantly the slump flow. This could point out that there is an optimal mixing time and that it was exceeded. Also, it is possible that there is a dependency of the mixing process on the optimal superplasticizer content. According to [8] overmixing can lead to an increase of the fraction of fine particles through abrasion. Therefore, more surface is created and the amount of superplasticizer must be increased to obtain a similar slump than without overmixing. The optimal SP content found in the experiments carried out could hence be only valid for the mixing procedure used for this thesis. Also, the value found is only valid for the specific SP used, it would hence have to be determined again if a different one was to be used.

The slump flow being optimised for a representative mix, it was decided that an effort would be made to link fibre size/width and fibre factor  $V_f$  with the slump flow and strength of casted prismatic samples.

### Workability over time

The tests of the decrease of workability were carried out with the HPFRC mix formula 13 (see Appendix, Figure A 1) that was going to be used for the final end-products, the table elements. During the casting of these elements, it is possible that the concrete cannot be processed immediately, so the goal was to have an estimation of the decrease of workability with time, as to know if the flowability of the concrete through the rather complex channels and geometries of the table elements. (Figure 33; Section 3.5) could be assured.

Figure 7 shows the decrease of the slump diameter with time. After 4 hours and 15 min the slump diameter of the mix, which wasn't remixed before every slump flow test, had a slump diameter reduced by 36% compared to an initial slump diameter of 26.25 cm. The other mix

with remixing for 1 min on the Hobart A200N on speed 1 before every test had at the same time a reduced slump diameter by 49 % compared to an initial slump diameter of 26.38 cm.

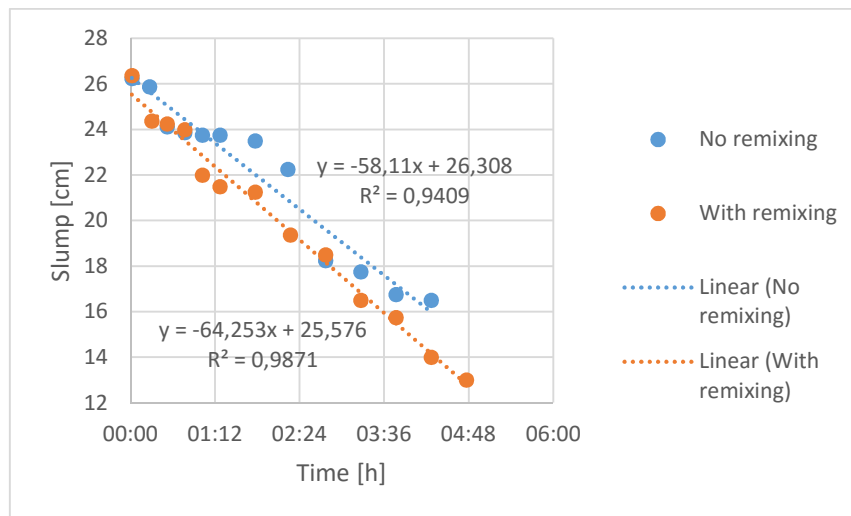


Figure 7: Decrease of slump diameter over time.

Initially it was expected that the mix which was remixed before every slump would remain more workable than the mix which wasn't remixed. Especially because the remixing would reverse any thixotropic build-up [3]. The fact that the not remixed concrete mix loses its workability less, could also be the result of fibres being deformed or crooked with every mixing process of the remixed concrete. This could be verified by repeating the experiment but with two mixes which contain no fibres. If in this case the concrete which is remixed has a smaller loss of slump diameter than the one without remixing, then it is likely that the deformation of the fibres are responsible for this phenomenon. Else it could be linked to overmixing which was discussed above (see section "Optimal superplasticiser content for the mix").

### Isothermal calorimetry

The heat flow over time caused by the hydration reaction of the concrete matrix (formula 12, see Appendix, Figure A1) can be seen in Figure 8. Two main peaks are shown. The first peak is due to the rapid initial reaction of  $C_3A$  and the dissolution of calcium sulphate [3]. But as the isothermal calorimeter takes time to accomplish stable conditions the first hour is not very reliable. The second peak occurs after 15.5 hours and is mainly the result of the hydration of  $C_3S$  [3]. The acceleration phase starts here roughly after about 7 hours and ends at the peak which occurred after 15.5 hours.

According to [9] the setting time cannot be related directly to the heat of hydration because also binder, water and aggregates determine how advanced the hydration process needs to be in order to create enough rigidity. Hence, the setting time cannot be determined with certainty out of Figure 8. For conventional concretes with w/c ratios between 0.35-0.5, initial setting is typically at the beginning of the acceleration phase and the final setting close to the end of the acceleration phase [9]. Therefore, it is possible that the final setting time for the concrete matrix occurs somewhere near 15 h after adding the water to the mix.



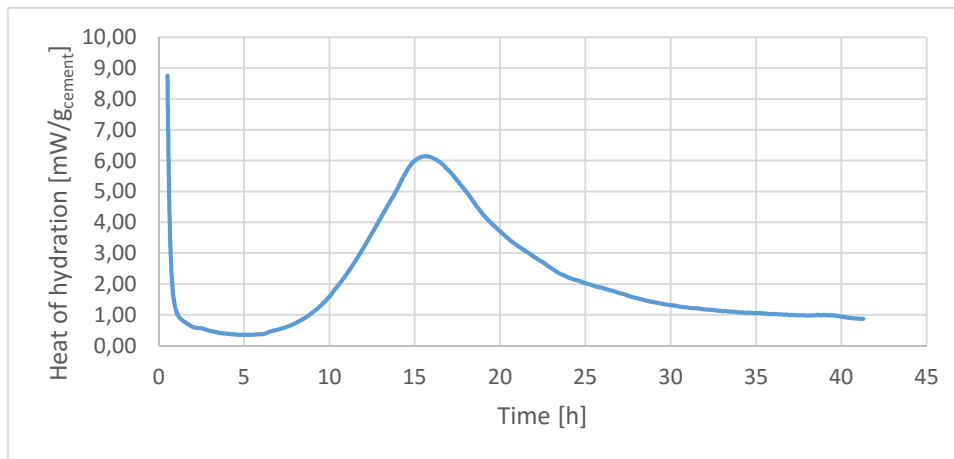


Figure 8: Heat of hydration in function of time.

Figure 9 shows the cumulative heat of hydration with time for the concrete matrix. For concrete and cement it is often favoured to reduce the amount of released heat in order to prevent thermal cracking. According to [10] steel fibres don't prevent thermal cracking but the usage of short fibres, like in this thesis, leads to smaller cracks which are more evenly distributed and can prevent that micro cracks turn into macro cracks, which is overall beneficial. Therefore, thermal cracking as well as shrinkage were not considered problematic for the HPFRC mixes.

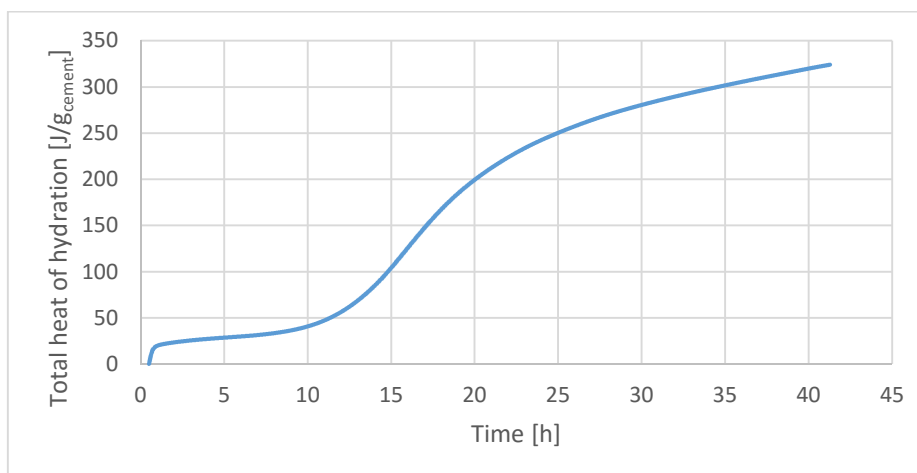


Figure 9: Cumulative heat of hydration over time.

## Bending and compression of HPFRC

In a first step the volume fraction of the different fibre types were set to be the same for all three fibre types, for reasons of comparison between the different types of fibres. Because the tests for finding the optimal superplasticizer were performed with 10x0.16 mm fibres and a volume fraction of 2.75 vol. %, the 6x0.15 mm and 13x0.16mm fibres were set to have the same volume fraction of 2.75 vol. %.

In a second step the volume fraction of the 6x0.15 mm and 13x0.16 mm fibres were varied in order to obtain a similar slump flow as for the 10x0.16mm with a volume fraction of 2.75 vol. %. The corresponding slump flow for the 10x0.16mm fibres and volume fraction of 2.75 vol. % was 26.25 cm. In the case of the 6x0.15mm fibres the volume fraction was increased to be 3.13 vol. % and the measured slump flow was 26.25

cm. In the case of the 13x0.16mm fibres the volume fraction was decreased to be 1.95 vol. % and the measured slump flow was 25.5 cm.

In Table 5 an overview is given over the different fibre types, their aspect ratio, volume fraction and fibre factor and the measured slump diameter. Moreover, the corresponding average flexural strength and average compressive strength after the bending and compression tests are shown in Table 5.

Fibre type	vol. [%]	Aspect ratio [-]	Fibre factor [-]	Slump diameter [cm]	Flexural strength [MPa]		Compressive strength [MPa]	
					7 Days	28 Days	7 Days	28 Days
none	-	-	-	28	7.36 ± 0.58	12.7 ± 0.03	80.4 ± 2.8	100 ± 8.0
6x0.15	2.75	40	1.1	27.5	26.8 ± 0.26	44.8 ± 1.6	103 ± 1.2	141 ± 2.6
	3.13	40	1.3	26.25	34.1 ± 1.2	42.9 ± 3.3	99.7 ± 2.4	142 ± 2.1
10x0.16	2.75	62.5	1.7	26.25	43.0 ± 0.30	52.8 ± 0.45	109 ± 2.1	151 ± 6.1
13x0.16	1.95	81.3	1.6	25.5	51.6 ± 3.5	51.7 ± 4.7	103 ± 1.1	131 ± 3.7
	2.75	81.3	2.2	22.75	63.1 ± 2.9	68.0 ± 3.2	113 ± 3.8	155 ± 2.7

Table 5: Overview over average flexural and compressive strength for different mixes [See Appendix, Figure A 1].

Figure 10 shows the average flexural strength after 7 and 28 days of different fibre types with the same volume fraction of 2.75 vol. %. Compared to the 6x0.15mm fibres the 28 days flexural strength is increased by 17.9%(10x0.16mm) respectively 51.8%(13x0.16mm). The increase of flexural strength could be explained by the fact that in this case mainly the length of the fibres was increased; due to the longer bond length of the fibres the required friction to be able to pull the fibres out of the matrix is higher. Also, the width of the cracks which can be bridged is larger. Additionally, it has been shown, e.g., by [11] that the force needed to pull steel fibres out of the cement matrix decreases with increasing diameter of the fibre (comparing same fibre lengths). These two facts are taken into account in the aspect ratio, or slenderness of the fibres  $f_{ar} = l_f/d_f[-]$  which multiplied by the fibre volume fraction  $V_f$  gives the fibre factor  $f_f = f_{ar} \cdot V_f$ . With an increasing fibre factor there is typically an increase in flexural strength (Figure 17). On a percentage basis the increase of flexural strength between 7 days to 28 days is the highest for the 6x0.15 mm fibres and is 67.2%. For the 10x0.16mm fibres the increase is 22.8% and for the 13x0.16mm fibres the increase is 7.77%.

Figure 11 shows the average compressive strength after 7 and 28 days for the different fibre types with the same volume fraction of 2.75 vol. %. Compared to the 6x0.15mm fibres the 28 days compressive strength is increased by 7.1% (10x0.16mm) respectively 9.9% (13x0.16mm)

The increase of compressive strength between 7 and 28 days is 36.9% for the 6x0.15mm fibres and 38.5 % for the 10x0.16mm fibres and 37.2% for the 13x0.16mm fibres.

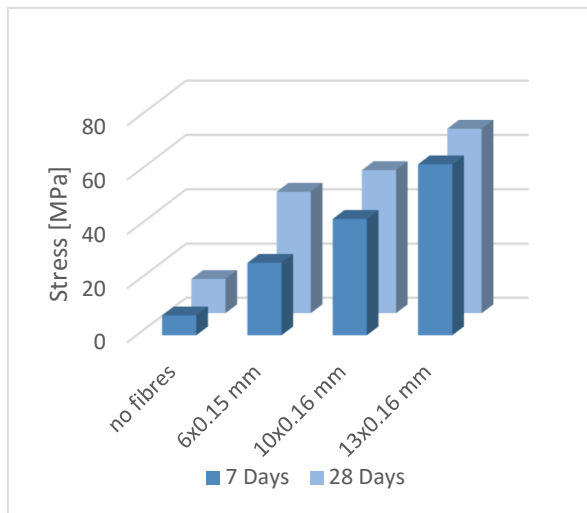


Figure 10: Flexural strength for different fibre types but with fibre contents of 2.75 vol. %.

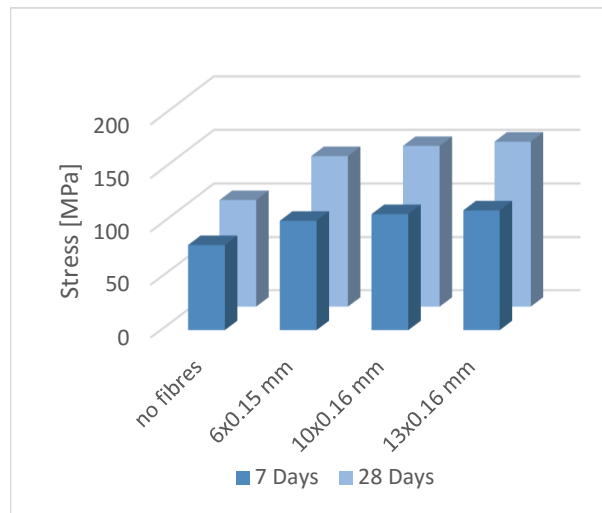


Figure 11: Compressive strength for different fibre types but with fibre contents of 2.75 vol. %.

Figure 12 shows the 7 and 28 days flexural strength for 13x0.16mm fibres with different volume fractions. The increase of 28 days flexural strength is 31.5% between an addition of 1.95 vol. % and 2.75 vol. % of fibres.

Figure 13 shows the 7 and 28 days compressive strength for 13x0.16mm fibres with different volume fractions. The increase of 28 days compressive strength is 18.3% between an addition of 1.95 vol. % and 2.75 vol. % of fibres.

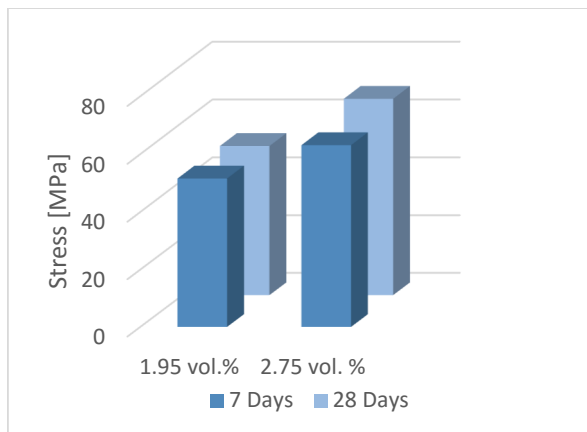


Figure 12: Flexural strength for 13x0.16mm fibres with varying fibre contents.

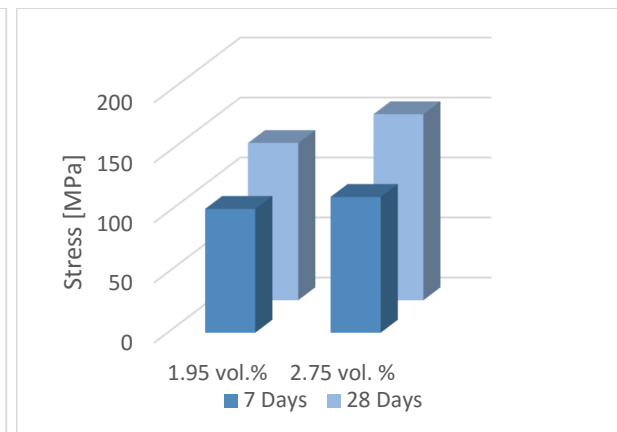


Figure 13: Compressive strength for 13x0.16mm fibres with varying fibre contents.

Figure 14 shows for the 6x0.15mm fibres a decrease of flexural strength of 4.4% with increasing volume fraction from 2.75 vol. % to 3.13 vol. %. It has to be noted that the amount of increased fibres was not very high and that these results are inside the standard derivation and the decrease of flexural strength is therefore not significant.

Figure 15 shows for the 6x0.15mm fibres an increase of 0.7% for the compressive strength. The result lies also inside the standard derivation but seems reasonable.

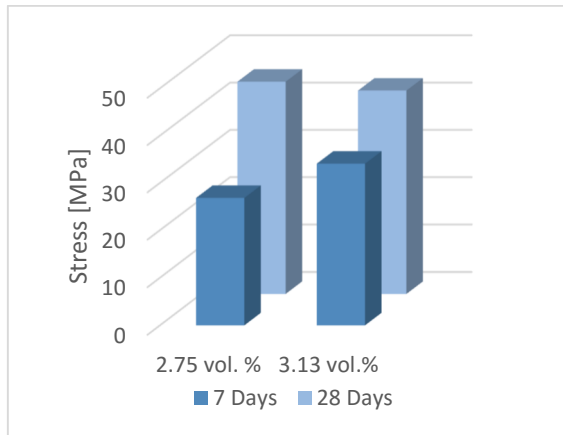


Figure 14: Flexural Strength for 6x0.15mm fibres, with varying fibre content.

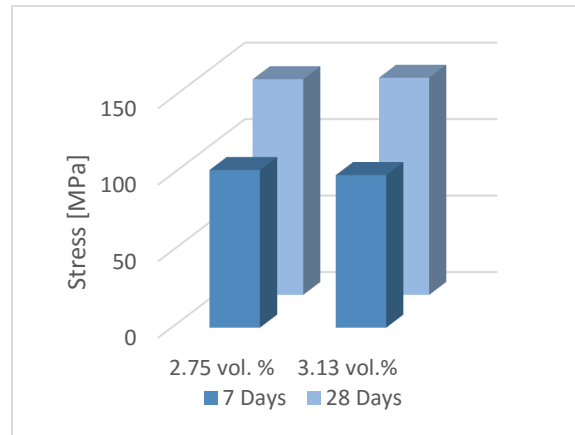


Figure 15: Compressive strength for 6x0.15mm fibres, with varying fibre content.

The results from the bending and compression tests must be viewed critically. Firstly, for every mix only three samples were used for obtaining the flexural strength and for the compressive test six samples were used. Three samples are a rather low amount for a statistical evaluation. Secondly, as shown by [6], 4-point bending tests deliver more accurate results with less fluctuation than 3-point bending tests for HPFRC. Thirdly and most important is the influence of the fibre orientation. According to [12] there are two main reasons for fibre orientation, shear induced orientation and wall effects. As the casted samples were small (4x4x16 cm) and the flow distance of the concrete small, the shear induced orientation might have a smaller influence than the wall effects. The wall effects however probably lead to an unneglectable overall overestimation of the flexural strength [6]. According to [12] the wall effects are of simple geometric nature and state that at a distance lower than  $L_f/2$  from the wall no fibre can be found perpendicular to the wall. Approximately the fibre orientation factor  $\alpha$  at a distance lower than  $L_f/2$  is 0.6 [12]. A fibre orientation factor of 0.5 stands for a perfect isotropic material and an orientation factor of 0 or 1 for fully anisotropic materials [13]. Therefore, the wall effects increase with longer fibres and for casted prisms, the influence of the wall effect has a higher impact on the flexural strength, the smaller the height and width of the sample is.

Most standards therefore propose bigger dimensions for the prisms than the 4x4x16 cm used here. For example, the standard for fibre reinforced concrete SIA 162-6 suggests the dimensions 10x10x60cm for prisms. However, due to the tight schedule of the project as well as the test machine and out of the convenience of already having the necessary moulds, the decision had been made of using 4x4x16 cm prisms. One benefit of this is, that the dimensions of the 4x4x16 cm prisms are closer to the actual dimensions of the channels and tubes for the end-product (table element).

The results make it possible to do a relative comparison of compressive and flexural strength between the different HPFRC mixes with different fibre contents and fibre types, and are therefore useful for the mix design.

### **Influence of the fibre factor $f_f$ on the strength and workability**

As seen above, a way to relate the flexural and compressive strength to the aspect ratio of steel fibres and their volume fraction is the fibre factor  $f_f$  [6]. In Figure 16 the slump flow is shown in function of the fibre factor. It can be seen that for an increasing fibre

factor the workability in terms of slump flow decreases. Figure 17 shows the 28 days flexural strength of all the mixes from Table 5 in function of the fibre factor. It can be seen that for an increasing fibre factor the flexural strength increases in an apparently linear manner. In Figure 18, the 28 days compressive stress is shown in function of the fibre factor. It can be seen that the compressive strength increases with increasing fibre factor in a linear manner. Similar trends between fibre factor and flexural strength as well as for fibre factor and slump flow have been observed by [6].

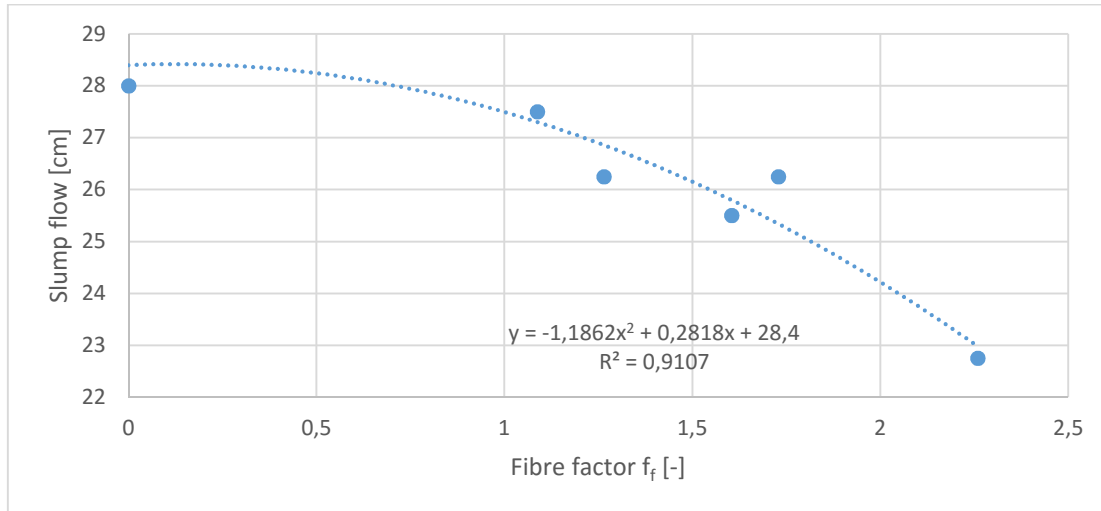


Figure 16: Fibre factor vs. slump flow.

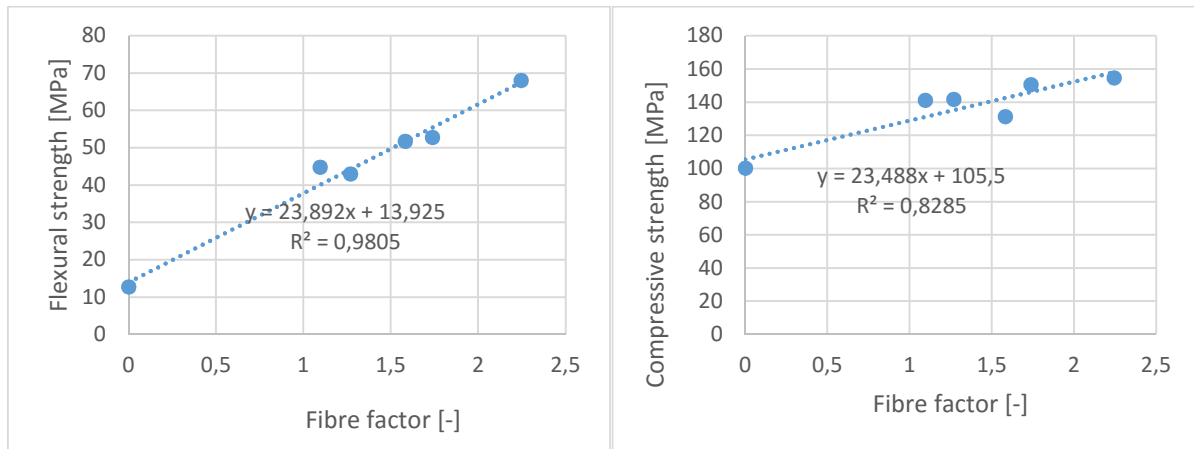


Figure 17: Fibre factor vs. flexural strength, 28 days.

Figure 18: Fibre factor vs. compressive strength, 28 days.

The results mentioned above provide a good basis for a first mix design and in this case enable to work more precisely towards the realisation of the wished end-product. Changing the fibre factor  $f_f$  affects the compressive, flexural and workability in a predictable way. The results therefore make it possible to know the limits of the mix and adapt it in terms of aspect ratio  $f_{ar}$  and volume fraction  $V_f$  of the fibres depending on the requirements.

These results can only be used directly for the concrete mix and the procedures mentioned in section 2.2, as variations in amounts, mixing time, and exact products used, can change the end result substantially. The knowledge of the existence of the relationships enables however after some testing to find again these relationships and apply them to new materials and mixing procedures.

Finally, it could be interesting for future research or projects to gather more data about the influence of the fibre orientation. The fibre orientation depends on the casting process as well as the type of fibres respectively the aspect ratio of the fibres and the fibre volume fraction [12]. Moreover, the fibre orientation is known to have a high influence on the mechanical properties of the hardened concrete. This could potentially enable a more precise determination of an optimal mix design for the future.

### **Strain hardening**

During the 7-days bending tests, a slight strain-hardening tendency was observed for the mix according to formula 14 (Figure A 1) with 13x0.16mm fibres and a volume fraction of 1.95%. The start of the strain hardening region can approximately be defined by the appearance of the first macro crack and the end where the maximum peak occurs [14]. Figure 19 shows the load displacement diagram after 7 days for the three tested samples from formula 16. After the appearance of the first crack the applied load could be increased by 24.5% (grey curve), 20.1% (orange curve) and 7.5% (blue curve). It has to be noted that the displacement was measured in terms of the distance which the machine (Walter + Bai) laid back. It was not possible to use an extensometer because of the tight schedule in the laboratory. However only a qualitative idea of the behaviour in the cracked state.

For the same formula 14, but after 28 days hardly any or no strain hardening could be observed. According to [15] for PVA fibres in SHCC aging of the material can lead to a more brittle behaviour due to the continued hydration process, and therefore the strain hardening region is less pronounced. This might also be valid for the usage of steel fibres in HPFRC.

In comparison to the concrete formula 14, with 13x0.16mm fibres and 1.95 vol. % the mixes with shorter fibres showed no particular strain hardening behaviour and behaved in a more or less brittle way. This could be explained that according to [14], strain hardening depends strongly on the cracks and the ability of the fibres to bridge those cracks. The 13mm long fibres can bridge larger cracks and are more effective in bridging macro cracks than the 6mm and 10 mm long fibres and therefore strain hardening should be more likely to observe.

In comparison to the formula 14, the concrete formula 10 with the same 13x0.16mm fibres and a higher volume fraction of 2.75 vol. % showed less or no strain hardening. It was initially expected that mixes according to formula 10 would more likely exhibit strain hardening, especially because of the higher fibre content. However, three out of six samples for formula 10 showed during the bending tests a fundamentally different crack pattern. A “shear-like” crack was formed from the location where the load was applied to the support. This crack pattern was not observed by the testing of any other mixes. This might be an indicator that for mix 10 shear could have a significant role. And perhaps 3 out of 6 samples might have failed due to shear force and not bending. This might have caused a more brittle behaviour.

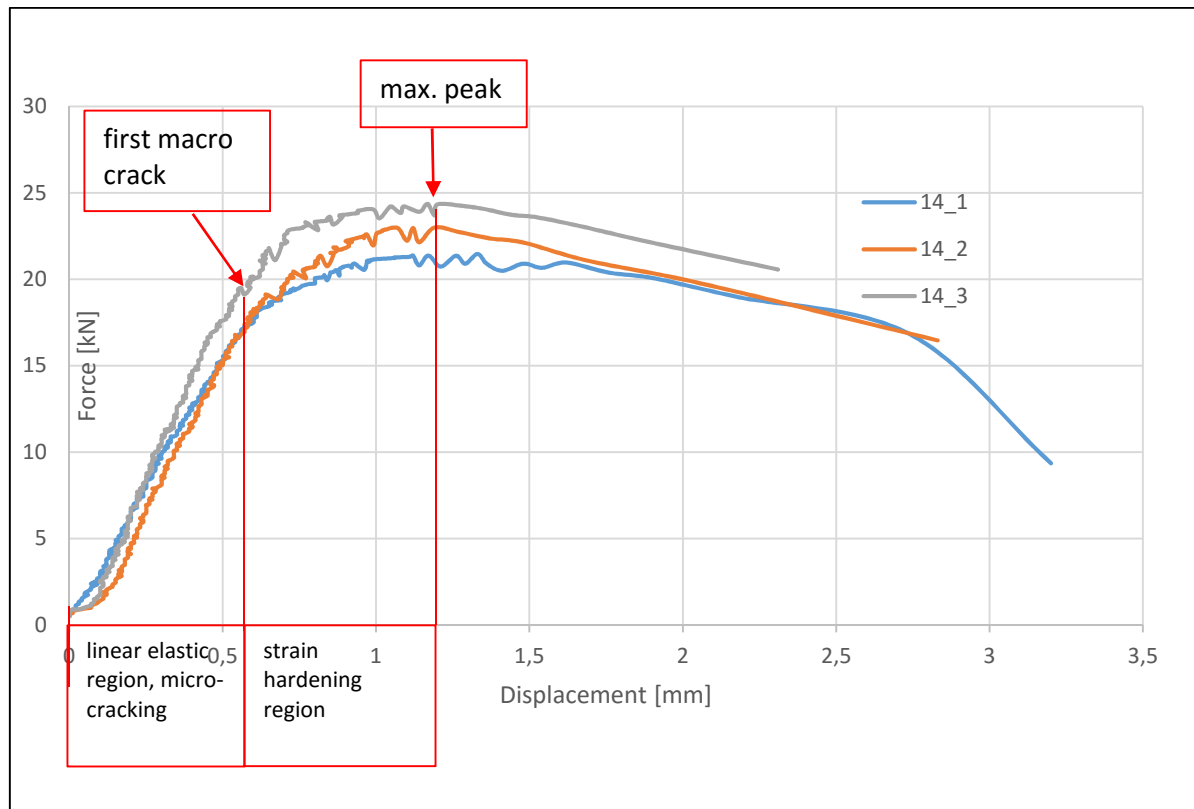


Figure 19: 7-days load displacement diagram for 13x0.16 mm fibres with 1.95 vol. %.

Overall it has to be noted that for strain hardening the influence of scale-effects is large [16] and the size of the tested specimen has a huge impact on the macro cracks and their width [16]. Due to the huge impact the size and geometry has on the strain hardening according to [17], strain hardening should not only be seen as a material characteristic but more as a structural characteristic. Therefore, the reason that strain hardening was even slightly observed for mix 14 by these low fibre contents, lies probably in the small geometric properties of the sample and possibly the fibre orientation which had been discussed in the previous section ("Bending and compression of HPFRC"). However, the dimensions of the 4x4x16 cm prisms are quite close to the geometric properties of the channels and tubes for the end-product (table element). Additionally, it has to be noted that strain hardening in a bending test does not automatically lead to strain hardening in tension [17].

The strain hardening behaviour still must be observed more in detail and could be a scope for future research because strain hardening and a ductile behaviour is most important for structural elements. Further investigation of strain hardening behaviour was beyond the scope of this project can could not be obtained in the short time given.

### 3.3 Mechanical properties of printed sand

Figure A 3 and Figure A 4 in the Appendix show the compressive and bending strength of sand printed elements. It can be seen that due to the fact that the sand-printed elements are printed layer by layer (section 2.1) the material is anisotropic and the mechanical properties depend on the direction of the applied load.

Due to the fact that the bending strengths of both binders are rather low and the wall thicknesses of the sand-printed elements were small, an additional constraint for the design of the table was a maximal height of 30cm. Apart from limiting the height, this



pressure issue could possibly be solved by exerting a counteracting pressure on the outside of the formwork by immersing the formwork in sand. A table using this technique was also designed and cast (see section below: “Wished End-product, Table Element”).

### 3.4 Interplay of printed sand and water

As mentioned in section 2.1, the formwork is made of sand and binder. There were suspicions that water might either interact with the binder in some way or water from the concrete matrix might be absorbed. It was hence decided to investigate the interaction of these formworks with water.

#### Preliminary testing

A first test was to fill sand-printed samples with water and see how fast the water flows through the matrix. Surprisingly, even though the speed of filling was rather rapid the water poured out as fast as it entered the element. This showed to be valid for both binders (see Figure 20 and Figure 21).



*Figure 20: Flowing of water through a sand-printed element (phenolic binder)*



*Figure 21: Flowing of water through a sand-printed element (furanic binder)*

It was suspected that the elements might have a high porosity, which would have to be investigated upon later. Additionally, the water seemed to be absorbed by the walls of the sand-printed elements throughout the experiment, which led to the suspicion that it would be worthwhile having a look at the sorptivity too.

A second preliminary test was to put printed elements for both binder types in water for some time and see if something particular could be noticed. Indeed, after some hours the elements lost strongly in cohesion and were very friable. Suspecting that some leaching might be going on, especially as an idea was that the sand-printed formworks could be wetted with water before casting (more water for hydration of the cement), it was decided to carry through a total carbon analysis to see if and how much of the binder left the matrix.



## Total Organic Carbon analysis

Preliminary observations could be made while handling sand-printed samples about a great loss of cohesion of the sand-printed material when in prolonged contact with water, and a high permeability and sorptivity of the material. This led to questions about the interaction of the sand-printed elements and the water contained in the concrete.

It was hence decided to at first investigate a possible leaching of the binder in the sand-printed elements when in contact with water, as the used binder are of organic nature. A TOC analysis has hence been carried through.

The analysis was carried through following the procedure described in section 2.2.2. The results can be seen in Table 6.

Binder type	Sample	Weight, before test [g]	Water added [g]	Time sample spent in the water	Total carbon [ppm]	Total organic carbon [ppm]	Inorganic carbon [ppm]
Phenolic	1	4.6634	23.3170	5 min	2.186	1.984	0.233
	2	3.2913	16.4665	60 min	2.550	1.928	0.622
	3	4.1281	20.6405	24 h	15.73	11.06	4.67
Furanic	4	3.8271	19.638	10 min	18.28	18.18	0.10
	5	3.0144	15.069	60 min	33.15	33.02	0.14
	6	6.3753	31.875	24 h	80.56	80.29	0.27
Reference value (container without sample)					1.382	1.274	0.1076

Table 6: Results of the total organic carbon analysis.

As seen, some leaching is going on. Since this seems to lead to a reduced strength of the formwork material which would eventually have to carry the load of the fresh concrete, it was decided to not pursue the idea of wetting the formwork with water before casting, and in general to avoid prolonged contact of the sand matrix with water.

## Sorptivity

As explained above, the apparent water intake and permeability of the sand-printed elements led to a desire to quantify these two behaviours. For this samples made of the sand-printed material were used for two types of binders (furanic and phenolic binder), and also samples where the surface has been impregnated using epoxy resin.

It can be seen in the case of the non-impregnated samples (Figure 22) that the speed of

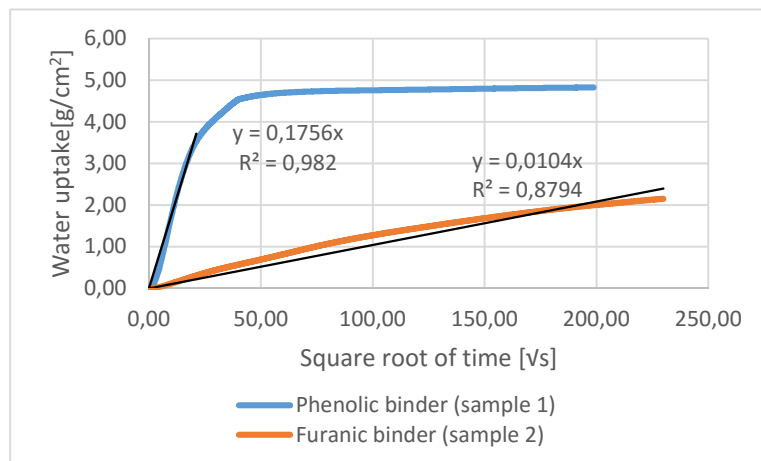


Figure 22: Water uptake of printed sand elements, non-coated.

water uptake in the beginning of the experiment is approximately 17 times higher for the printed element where a phenolic binder was used than for the one where a furanic binder was used. The sample with the phenolic binder reaches a plateau after about 28 minutes, possibly indicating that the water reached the top of the sample.

The fact that the blue curve for the phenolic binder continues to grow after  $38.7^2 = 1500$  seconds could possibly indicate the presence of at least another kind of pores, which would according to Equation 6 take more time to fill because of a smaller pore radius.

The fact that the orange curve is flatter than the blue one might analogously indicate that the sample using furanic binder either has smaller pores, lower porosity, a smaller wetting angle, or a smaller surface tension.

Figure 23 shows that both binders, when the surface is impregnated with epoxy resin, have a water uptake speed which is almost the same, with the furanic binder still being a tad slower. It must be noted though, that the total water uptake for the epoxy-coated samples after 40'000s is approximately 44 times lower (phenolic binder) and 18 times lower (furanic binder) than for the non-coated samples.

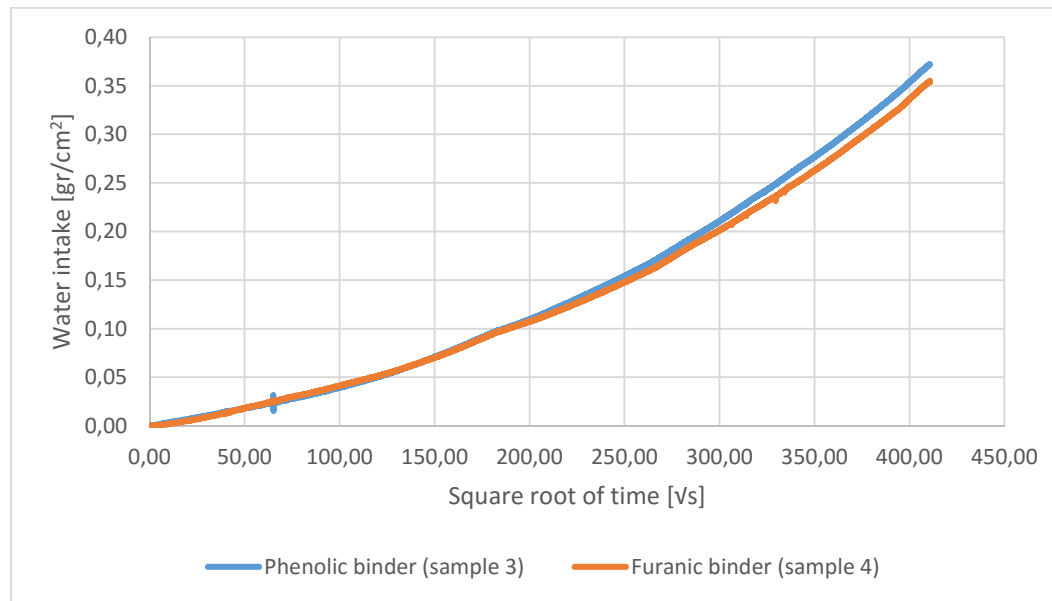


Figure 23: Water uptake of printed sand elements, coated with epoxy resin.

This difference in water uptake speed between coated and non-coated samples can be explained by the fact that in the case of the samples 3 and 4 the water, to get to the enclosed matrix on the inside of the samples, has first to go through the coating layer which seems to have either a low wetting angle, a small pore size, plainly low porosity (this will be investigated upon later in this section). This impregnation layer seems to be decisive for the rate of ingress of the water.

An additional implication of the presence of a fraction of the pores being smaller might be that according to Equation 12, the maximum height of capillary rise would be higher.

$$h_{max} = \frac{2 \cdot \gamma_{LV}}{r \cdot \rho \cdot g} \cdot \cos(\theta) \quad [7] \quad (12)$$

The implications of the observations are that the water intake would be a factor to take into account for further research and application in real-world scenarios. A high sorptivity in both cases might lead to a proclivity to humidity of sand-printed elements if contact with water is possible, which could have deleterious effects on serviceability:

- Possibly corrosion issues for the fibres if usage of concrete with higher W/C ratio where presence of capillary pores could enable the transport of the humidity and

air, necessary for the corrosion reaction to occur. In the case of the mix used for this thesis, the low W/C ratio would lead to a low presence of capillary pores, which means that corrosion may only happen in the surface fibres.

- Transport of humidity to nearby structural elements that are more sensitive to water (wood, steel...)
- Possible long-term effect on the strength and form of the sand.

These effects are though speculative and would necessitate further investigation. It was decided to use the furanic binder instead of the phenolic binder as we could thereby possibly limit problems that might be related to water absorption.

It is unclear whether the sorptivity of the sand formworks means that the water contained in the concrete mix would get absorbed in some way. Nothing particular was noticed during the experiments. The subject was however not properly investigated and could be investigated if needed in a future study.

## Porosity

It was decided, so as to get more data about the high apparent porosity, to measure the porosity of a non-coated sand-printed cube, a coated sand-printed cube (epoxy coating), and a thin platelet cut from the surface of a coated cube (to know the porosity of the impregnated part of the coated cube). All sand elements were printed using furanic binder.

The measurements of weights and dimensions obtained through the method described in section 2.2.2 can be seen in Table 7. The derived bulk/matrix densities and porosities can be seen in Table 8.

Sample	Dry weight [g]	Wet weight [g]	Water weight [g]	Dimensions [mm]			Vol. [mm <sup>3</sup> ]
Coated platelet	4.8560	5.1410	0.2850	1.40	49.60	49.90	$3.47 \cdot 10^3$
Non-coated cube	169.3692	225.2783	55.9091	50.20	49.95	50.20	$125.9 \cdot 10^3$
Coated cube	177.3057	225.7121	48.4064	50.45	50.40	50.10	$127.4 \cdot 10^3$

Table 7: Weights and dimensions of the samples used for the porosity calculations (only furanic binder).

Sample	$V_b$ [mm <sup>3</sup> ]	$V_s$ [mm <sup>3</sup> ]	$\rho_b$ [kg/m <sup>3</sup> ]	$\rho_b$ [kg/m <sup>3</sup> ]	Porosity $\Phi$ [-]
Coated platelet	$0.285 \cdot 10^3$	$3.18 \cdot 10^3$	$1.53 \cdot 10^3$	$1.40 \cdot 10^3$	8.22%
Non-coated cube	$54.91 \cdot 10^3$	$69.97 \cdot 10^3$	$2.421 \cdot 10^3$	$1.345 \cdot 10^3$	44.42%
Coated cube	$48.41 \cdot 10^3$	$78.98 \cdot 10^3$	$2.244 \cdot 10^3$	$1.392 \cdot 10^3$	38.00%

Table 8: Porosity of the sand printed elements, and bulk/matrix density (only furanic binder).

The porosity of the coated platelet is a lot lower, consistently with what has been discussed above when investigating the sorptivity (see Figure 23). Also consistent is the high porosity of the non-coated cube and the tad lower porosity of the coated cube.

## Conclusions/Decisions

The phenomena observed above laid ground to the question if the sorptivity, porosity, and loss of cohesion (when in prolonged contact with water) of the sand-printed elements could be sources of problems in the future.

Cuts through some prototypes for the table were made, to have a look at how well the infilling goes (entrapped air, bubbles?), but also to see if any problems could be seen. The interface seemed fine, and no other issue could be noted (Figure 24 and Figure 25).

However, it is clear that the porosity might be beneficial: Entrapped air and bubbles in the concrete could possibly escape the formwork through the high porosity, which is given the possibly intricacy of these formworks something that would be advantageous.

To minimise problems due to the sorptivity, it could be else productive to coat sand-printed elements with epoxy resin. This might though hinder entrapped air from escaping the sand-printed formworks.



Figure 24: Prototype for the table, cross section 1.



Figure 25: Prototype for the table, cross section 2.

Concerning the binder, it was decided to use the furanic one as the sorptivity rate for this binder is lower, which renders less probable that problems could be caused by influx of water. The point of choice of the exact binder could however be investigated more into detail in further research.

### 3.5 Casting of prototypes for the wished end-product

#### Straight tubes

For the filling of tubes with small diameters, the length of the fibres together with the volume fraction of fibres can be a limiting factor. To study this behaviour and have a recommendation for the minimal diameters for the tubes and channels for the end product (Table element) straight tubes were vertically filled.

Table 9 shows the different sand printed tube diameters which can be filled with different mixes. Classified as green are diameters which can be filled easily and show no or only marginal defects namely cavities, in the longitudinal cut. Classified as red are diameters which cannot be filled at all. Orange are diameters which can be filled but show cavities especially at the interface between the sand printed structure and the concrete.

Fibre type & Volume Fraction	Tube Diameter[mm] Slump flow [cm]	50.87	39.77	30.92	23.85	18.22	13.73	10.14	7.28	5
None	28.00 cm	✓	✓	✓	✓	✓	✓	✓	x	x
6x0.15mm 3.13 %	26.25 cm	✓	✓	✓	✓	✓	x	x	x	x
10x0.16mm 2.75 %	26.25 cm	✓	✓	✓	~	~	x	x	x	x
13x0.16 1.95 %	25.50 cm	✓	✓	✓	~	x	x	x	x	x

Table 9: Fillability of different tube diameters with different fibre types.

Figure 26 shows the sand printed tubes filled with HPFRC containing 6x0.15 mm fibres, the tubes which could be filled show no big cavities. Figure 27 shows the same but with

10x0.16 mm fibres, the tube with a diameter of 18.22mm shows a high amount of cavities at the interface. The tube with a diameter of 23.85 mm shows a few bigger cavities, Figure 28 shows the tubes filled with HPFRC and 13x0.16mm fibres. The tube with a diameter of 23.85 shows some bigger cavities and a cavity at the interface (Figure 5).

From these results the general recommendation would be to have the diameter of the sand-printed tubes at least three times bigger than the length of the fibres and for curved tubes and partially horizontal tubes four times bigger.



Figure 26: Straight tubes, 6x0.15mm fibres.



Figure 27: Straight tubes, 10x0.16mm fibres.



Figure 28: Straight tubes, 13x0.16 mm fibres.

### **L-shaped tubes with varying angles**

In Figure 29 the results and the flowing behaviour can be seen for the L-shaped tubes with the usage of different fibre types. The 6x0.15mm fibres with a slump flow of 26.25 cm could fill the tubes with a diameter of 2 cm and varying angles without problems. The 10x0.16mm and 13x0.16mm fibres with a slump flow of 26.25cm respectively 25.5 cm did not pass the angle section.

As the table prototype and the desired end-product would have complex geometries and tubes and channels of varying diameter and curvature, it was decided - based on the latter two experiments - that the mix for the table element would be Formula 13 with 6x0.15mm fibres and a volume fraction of 3.13 %.

It would be also interesting, seeing that the concrete was not able to flow that far after the angle, to test the maximum flow length of concrete in straight tubes. A design possibility for the test would be to set an inner diameter of these tubes of 2cm, a length of 50cm, and either set an angle of, e.g., 45° or vary the angle to know the influence of the angle. Data of such an experiment could make it easier to predict if the concrete used can really fill all the voids of a sand-printed formwork.



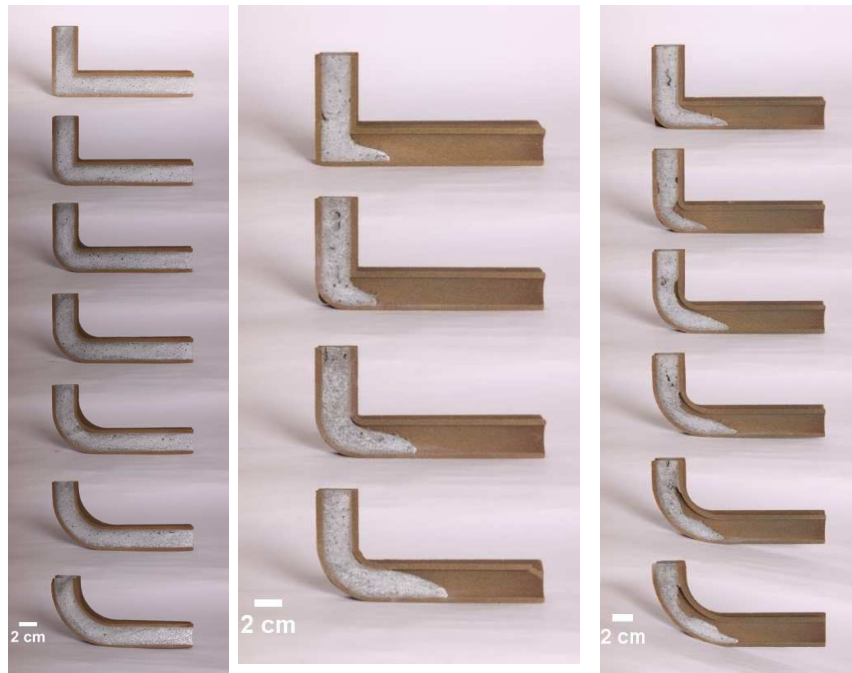


Figure 29: L-shaped tubes with varying bending radii, left 6x0.15mm fibres; middle 10x0.16mm fibres; right 13x0.16mm fibres. Bending radii (left picture), from top to bottom [mm]: 0,10,20,30,40,50,60. Arms on both sides of each L-shaped tube were originally 15cm long.

### Wished End-product, Table Element

The end product of this thesis was supposed to be an object which could showcase the possibilities for 3D sand-printed fibre reinforced high performance concrete hybrid structures.

To see if problems would possibly be encountered, some prototypes for the tables were designed and cast (see Figure 24, Figure 25, Figure 30, and Figure 31).



Figure 30: Prototype for the table, cross-section, 3.



Figure 31: Prototype for the table, cross-section, 4.

No problems could be observed on the cross sections (apart of some air bubbles and entrapped air on the third figure, due to a problem with the used batch on the mixing day, which had a significantly lower slump diameter than expected):

- No entrapped air nor bubbles, all void had been filled
- Sand/Concrete interface seems unproblematic

The table design was then implemented, produced, and cast in two variations:

- The formwork as can be seen in Figure 32 and Figure 33, which was painted in white and used directly for an exhibition.
- The same formwork, but embedded in sand (to counter the pressure exerted by the concrete on the inside of the formwork), lying in a “case” made of 3D-printed sand. This prototype still to the day of submission of the thesis lies in the sand case, as there was, given the tight time schedule, unfortunately no time to take care of removing the 3D-printed sand case and the loose sand.

Both tables were coated with epoxy coating where possible.



*Figure 32: Produced table, casted and coloured, view from the side.*

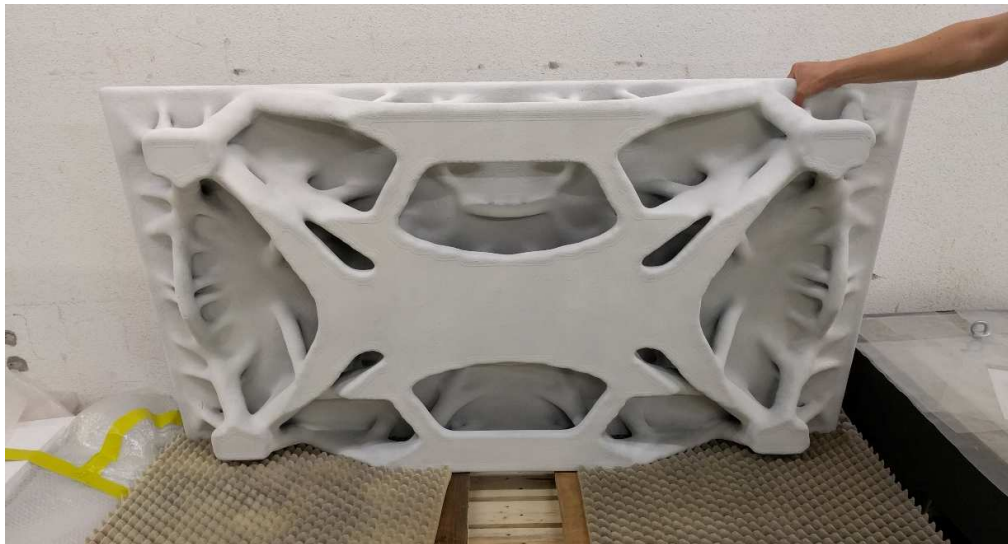


*Figure 33: Produced table, casted and coloured, view from below.*

A new possible problem emerged before casting: some loose sand was still in the formwork. It took some time, using a vacuum cleaner, to remove all visible volumes of sand. After casting it was though possible to hear when tapping gently on some spots of the prototype sounds indicating possibly that there is no concrete. It is not known at this point if these sounds show a flow problem of the concrete, a presence of loose sand, or if they are just misleading. It has still to be decided how the filling will be checked (e.g., cutting).

## 4 Conclusion

Very interesting results have been obtained in this explorative effort at realising 3D sand-printed high-performance fibre-reinforced hybrid structures.

Concerning the concrete mix itself:

- A first working HPFRC-mix fulfilling the absolute minimum requirements in terms of workability for this project has been found. A method of finding an optimal superplasticiser dry extract content for improving workability has been found, and could be used for other superplasticisers or other mixing procedures.
- A most probably reproducible direct link between fibre factor, slump diameter, and strength of the concrete has been found. This makes it possible for any given mix, when the measurements have been made, to adapt, e.g., the amount of fibres to increase workability or to increase strength while knowing what impact this change has on the other parameter. It might make sense though to add more data points to be able to divide the summarising “fibre factor” into “fibre aspect ratio” and “fibre volume fraction”, which might make it possible to control even more precisely the workability and strength. 3 mixes were designed, which differed only by the length, width, and mix volume fraction of the fibres (13mm, 10mm, and 6mm fibres). A slight strain hardening could be observed for some settings.
- The decrease of workability with time of the HPFRC – important fact to take into account as mixes eventually have to wait before getting casted - has been quantified. It has been observed that remixing a mix before casting is – surprisingly – actually worse for the workability than not remixing. This could be due to crooking of the fibres during the mixing, it would hence make sense to reproduce the experiment with mixes containing no fibres.
- Calorimetry testing showed that the used superplasticiser (BASF MasterGlenium ACE 30) has a rather limited retarding effect regardless of the rather high amount used in the formulas.

Concerning the sand-printed elements (without concrete):

- A not complete but still significant loss of cohesion of the printed sand elements when in prolonged contact with water has been observed. This could be linked to leeching of the binder.
- The sand elements made with the phenolic binder and the furanic binder both show a high sorptivity, with the phenolic binder elements having higher one. When samples are coated with epoxy coating, the sorptivity diminishes by a lot.
- A high porosity (44%) of the sand elements could be found (for the ones using furanic binder, which were the only ones investigated upon). A lower porosity (8%) could be found for samples coated with epoxy coating.
- The epoxy coating seems to be a good way of reducing the probability of problems through lesser intake of water.
- The high porosity might actually be helpful by providing a possibility for entrapped air and air bubbles to escape the sand-printed formwork when casting concrete.



Concerning the printed-sand/concrete hybrid structure:

- The shortest fibres (6mm) have been chosen during for the final mix of this thesis as the resulting workability was the best. Strain hardening as wished might although be harder to achieve with these fibres as the aspect ratio is rather low ( $f_{ar} = 40$ ). In that sense, it might be useful to have a look at fibres with a higher aspect ratio. If bigger fibres are necessary, it would also be most probably also necessary to increase the size of the cross section of all channels of the formworks.
- Prototypes for the wished end-product, the topologically optimised sand-printed table serving as a showcase model for the possibilities of the technology, were cast. No significant issues could be noted, and no entrapped air or bubbles could be seen on the cut cross-sections. The only issue experienced was presence of entrapped air in a sample due to a problematic batch which didn't flow as expected (smaller slump diameter).
- The table was printed and cast, and has to be analysed in depth to see whether all voids have been filled. There might still be a problem do to the possible presence of inaccessible loose sand in the formwork, and it could be possible that the concrete could not flow to all points of the void inside of the formwork. More (if possible non-destructive) testing on the table has to be decided in order to investigate that.

Finally, tests in the final stage of the bachelor thesis on another, more modern superplasticiser (BASF MasterGlenium SKY 561) showed a spread diameter approximately 14% higher than for the superplasticiser mainly used in this thesis (BASF MasterGlenium ACE 30) when using no fibres. Varying the superplasticiser dry extract content for the mix when using the new SP showed that it is possible to increase even more the workability, which would be useful for future applications (See Figure A 2 in the appendix).

## 5 References

- [1] Voxeljet, „Sandprinting,“ [Online]. Available: <http://www.voxeljet.de/services/sand/>. [Zugriff am 22 05 2016].
- [2] BASF, „Master Builders Solutions,“ [Online]. Available: <https://www.master-builders-solutions.basf.ch/de-ch/produkte/masterglenium/675>. [Zugriff am 16 Mai 2016].
- [3] R. J. Flatt, Materials I Skript: cementitious materials, ETH Zurich, 2015.
- [4] Sika, „Hochleistungsfließmittel,“ [Online]. Available: <http://deu.sika.com/de/gypsum-mortar-redirect/Trockenm%C3%B6rtel%20und%20Gipstechnologie/gypsum-product-groups/superplasticizers.html>. [Zugriff am 16 Mai 2016].
- [5] B. Research, „High Performance Concrete (HPC),“ [Online]. Available: <http://www.buildingresearch.com.np/newfeatures1.php>. [Zugriff am 16 Mai 2016].
- [6] P. S. & J. v. M. Mier, „Three-fibre-type hybrid fibre concrete,“ Institute of building materials, ETHZ, Zürich, 2004.
- [7] M. B. Dan, Materials, Technologies and Practice in Historic Heritage Structures, Dordrecht: Springer Science+Business Media B.V, 2010.
- [8] G. D. S. V. B. J. Dils, „Influence of mixing procedure and mixer type on fresh and hardened properties of concrete: A review,“ in *Materials and Structures 45(11)*, Rilem, 2012.
- [9] R. S. B. L. Karen Scrivener, A Practical Guide to Microstructural Analysis of Cementitious Materials, Taylor & Francis Inc, 2015.
- [10] B. Wietek, Stahlfaserbeton - Grundlagen und Praxisanwendung, Teubner Verlag, 2010.
- [11] T. Stengel, Verbundverhalten und mechanische Leistungsfähigkeit von Stahlfasern in ultrahochfestem Beton, München: TU München, Lehrstuhl für Baustoffkunde und Werkstoffprüfung, 2013.
- [12] L. Martinie and N. Roussel, “Simple tools for fiber orientation prediction in industrial practice,” *Cement and Concrete Research*, October 2011.
- [13] L. Martinie, J.-F. Lataste et N. Roussel, «Fiber orientation during casting of UHPFRC: electrical resistivity measurements, image analysis and numerical simulations,» *Materials and Structures*, April 2015.
- [14] J. W. J. v. M. I. Markovic, „Development of high performance hybrid fibre concrete,“ in *PRO 30: 4th International RILEM Workshop on High Performance Fiber Reinforced Cement Composites*, RILEM Publications S.A.R.L., 2003.

- [15] G. v. Zijl, Durability of Strain-Hardening Fibre-Reinforced Cement-Based Composites, Rilem, 2011.
- [16] P. Rossi, „Ultra-High Performance Fibre Reinforced Concretes: An Overview,“ in *PRO 15: 5th RILEM Symposium on Fibre-Reinforced Concretes (FRC) - BEFIB' 2000*, RILEM publications S.A.R.L, 2000, pp. 87-100.
- [17] J.-M. H. Mari Bøhnsdalen Eide, „Ultra High Performance Fibre Reinforced Concrete - State of the art,“ SINTEF Building and Infrastructure , 2012.
- [18] CIMbéton, „3.5 - Les Bétons Fibrés à Ultra hautes Performances - BFUP,“ in *Les bétons : formulation, fabrication et mise en oeuvre*, 2013, p. 135.
- [19] V. Morin, F. Cohen Tenoudj, A. Feylessoufi und P. Richard, „Superplasticizer effects on setting and structuration mechanisms of ultrahigh-performance concrete,“ *Cement and Concrete Research*, January 2001.
- [20] L. Martinie, P. Rossi and N. Roussel, “Rheology of fiber reinforced cementitious materials: classification and prediction,” *Cement and Concrete Research*, February 2009.
- [21] E. Denarié, D. Jacomo, N. Fady und D. Corvez, „Rejuvenation of maritime signalisation structures,“ 2013.

## 6 Appendix

Trial formulas	Form. 1	Form. 2	Form. 3	Form. 4	Form. 5	Form. 6	Form. 7	Form. 8	Form. 9	Form. 10	Form. 11	Form. 12	Form. 13	Form. 14	Form. 15	Form. 16	Form. 17	Form. 18	Form. 19			
Cement*	1	1	1	1	1	1	1	1	1	1	1	1	1	1	1	1	1	1	1			
Sand 0.1-0.45 *	1437	0.755	0.755	0.755	0.755	0.755	0.755	0.755	0.755	0.755	0.755	0.755	0.755	0.755	0.755	0.755	0.755	0.755	0.755			
Silica flour*	0.303	1000	1000	1000	1000	1000	1000	1000	1000	1000	1000	1000	1000	1000	1000	1000	1000	1000	1000			
Silica fume*	0.324	0.125	0.125	0.125	0.125	0.125	0.125	0.125	0.125	0.125	0.125	0.125	0.125	0.125	0.125	0.125	0.125	0.125	0.125			
SP*	0.04745	0.06762	0.08423	0.10108	0.11792	0.13477	0.09265	0.09265	0.09265	0.09265	0.09265	0.09265	0.09265	0.09265	0.1983	0.1983	0.13072	0.15251	0.14161			
Water	#####	#####	#####	0.07108	#####	#####	0.06515	0.06515	0.06515	0.06515	0.06515	0.06515	0.06515	0.06515	0.06515	0.06515	0.06515	0.06515	0.06515			
Dry Extr.	0.01408	#####	#####	#####	#####	#####	#####	0.02750	0.02750	0.02750	0.02750	0.02750	0.02750	0.02750	0.02750	0.02750	0.02750	0.03000	0.03500			
SP type	(SP 1)***	(SP 1)***	(SP 1)***	(SP 1)***	(SP 1)***	(SP 1)***	(SP 1)***	(SP 1)***	(SP 1)***	(SP 1)***	(SP 1)***	(SP 1)***	(SP 1)***	(SP 1)***	(SP 1)***	(SP 2)***	(SP 2)***	(SP 2)***	(SP 2)***			
Fibres*	0.225	0.550	0.325	0.325	0.325	0.325	0.325	0.325	0.325	0.325	0.406	0.000	0.373	0.227	0.373	0.373	0.373	0.373	0.373			
Fibre type	(2)****	(2)****	(2)****	(2)****	(2)****	(2)****	(2)****	(2)****	(1)****	(3)****	(1)****	-	(1)****	(3)****	(1)****	none	(1)****	(1)****	(1)****			
Water*	0.197	0.300	0.288	0.276	0.265	0.253	0.282	0.282	0.282	0.282	0.282	0.282	0.282	0.282	0.255	0.255	0.247	0.230	0.238			
Resultat water amoun	0.231	0.347	0.347	0.347	0.348	0.347	0.347	0.347	0.347	0.347	0.347	0.347	0.347	0.347	0.347	0.347	0.348	0.348	0.347			
W/B	0.174	0.309	0.309	0.309	0.309	0.309	0.309	0.309	0.309	0.309	0.309	0.309	0.309	0.309	0.309	0.309	0.309	0.309	0.309			
W/C	0.231	0.347	0.347	0.347	0.347	0.347	0.347	0.347	0.347	0.347	0.347	0.347	0.347	0.347	0.347	0.347	0.347	0.347	0.347			
Slump diam. [cm]	**	14.75	23.75	26.00	25.25	23.90	26.00	26.25	27.50	22.75	25.00	28.00	26.25	25.50	29.75	30.25	30.75	28.75	29.38			
Density***** [kg/m³]								2413	2375	2399		2243	2428	2352								
Fibre vol. fraction [%]								2.78	2.74	2.76		-	3.17	195								
Fibre factor [-]								174	109	224		-	127	158								
Flex. strength [MPa]																						
7 days								43.0±0.30	26.8±0.26	63.1±2.9		7.36±0.58	34.1±1.2	516±3.5								
28 days								52.8±0.45	44.8±1.6	68.0±3.2		12.7±0.03	42.9±3.3	517±4.7								
Compr. strength [MPa]																						
7 days								114±2.1	103±1.2	113±3.8		80.4±2.84	99.7±2.4	103±1.1								
28 days								151±6.1	141±2.6	155±2.7		100±8.0	142±2.1	131±3.7								
								*	amount given in mass / cement mass									type	length	width		
								**	stiffness too high for testing									****	Fibre types	(1)	6mm	0.15mm
																			(2)	10mm	0.16mm	
																			(3)	13mm	0.16mm	
								***	SP types	(SP1)	BASF MasterGlenium ACE 30											
										(SP2)	BASF MasterGlenium SKY 56								*****	measured through weight		

Figure A 1: All tested mixes and overview of their properties.

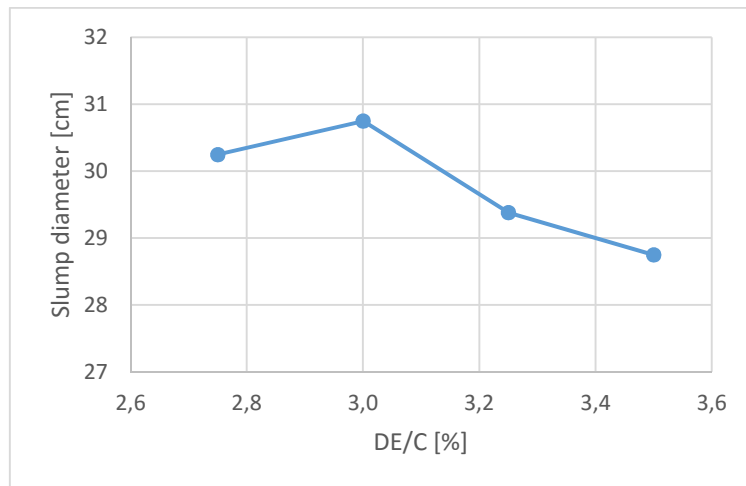


Figure A 2: SP dry extract content VS slump diameter, SP=BASF MasterGlenium SKY 561.

Compression	Coated? (Epoxy resin)	Axis	Compressive strength [MPa]		
			Average	StdDev	Overall Average
Furanic	no	X	8.00	0.216	8.37
	no	Y	7.65	-	
	no	Z	9.47	0.544	
	yes	X	12.57	1.144	12.80
	yes	Y	12.43	0.464	
	yes	Z	13.40	0.860	
Phenolic	no	X	6.60	0.163	8.56
	no	Y	10.00	0.082	
	no	Z	9.07	0.189	
	yes	X	10.37	0.170	12.32
	yes	Y	13.37	0.309	
	yes	Z	13.23	0.249	

Figure A 3: Compr. test results of sand-printed samples (preliminary tests by Dr. Timothy Wangler).

Bending	Coated? (Epoxy resin)	Axis	Bending strength [MPa]		
			Average	StdDev	Overall Average
Furanic	no	X	3.40	0.163	2.97
	no	Y	3.20	0.082	
	no	Z	2.30	0.141	
	yes	X	7.20	0.082	6.49
	yes	Y	6.50	0.327	
	yes	Z	5.77	0.694	
Phenolic	no	X	2.07	0.047	2.93
	no	Y	5.07	0.170	
	no	Z	1.67	0.047	
	yes	X	?		8.86
	yes	Y	10.37	0.899	
	yes	Z	?		

Figure A 4: Bending test results of sand-printed samples (preliminary tests by Dr. Timothy Wangler).

Density	Coated? (Epoxy resin)	Density [kg/m <sup>3</sup> ]
Binder type		
Furanic	no	1414
	no	
	no	
	yes	1458
	yes	
	yes	
Phenolic	no	1323
	no	
	no	
	yes	1389
	yes	
	yes	

Figure A 5: Density of sand-printed samples (preliminary tests by Dr. Timothy Wangler).

Components	$\rho$ [kg/l]	Mass [kg] per m <sup>3</sup>	Volume [l] per m <sup>3</sup>
<b>Powders</b>		1851.2	659.7
Cement (Lafarge)	3.150	642.8	204.1
Silica fume (ELKEM)	2.200	80.3	36.5
Limestone filler (Durcal 15)	2.700	642.8	238.1
Sand	2.680	485.3	181.1
<b>Water added</b>	1.000	192.8	192.8
Steel Fiber (BEKAERT 10/16)	7.850	353.3	45.0
<b>Sika Extender (SE)</b>	0.980	3.9	3.9
<b>Superplasticizer (SP)</b>	1.060	51.4	48.5
Dry extract 25.0	[%]	12.9	
Water part 75.0	[%]	38.6	38.6
<b>Water total</b>	1.000	231.4	231.4
<b>Air</b>			50.0
<b>Total</b>		2452.5	1000.0
	Spec. Weight	2452.5	

Figure A 6: Original mix recipe from Dr. Emmanuel Denarié.